

A Spatio-Temporal Dirichlet Process Mixture Model on Linear Networks for Crime Data

Sujeong Lee¹, Won Chang³, Jorge Mateu⁴, Heejin Lee⁵, and Jaewoo Park^{1,2}

¹Department of Statistics and Data Science, Yonsei University, Seoul, Republic of Korea.

²Department of Applied Statistics, Yonsei University, Seoul, Republic of Korea.

³Department of Statistics, Seoul National University, Seoul, Republic of Korea.

⁴Department of Mathematics, University Jaume I, Castellón, Spain.

⁵Department of Criminal Justice and Criminology, Sam Houston State University, Huntsville, USA.

January 16, 2025

Abstract

Analyzing crime events is crucial to understand crime dynamics and it is largely helpful for constructing prevention policies. Point processes specified on linear networks can provide a more accurate description of crime incidents by considering the geometry of the city. We propose a spatio-temporal Dirichlet process mixture model on a linear network to analyze crime events in Valencia, Spain. We propose a Bayesian hierarchical model with a Dirichlet process prior to automatically detect space-time clusters of the events and adopt a convolution kernel estimator to account for the network structure in the city. From the fitted model, we provide crime hotspot visualizations that can inform social interventions to prevent crime incidents. Furthermore, we study the relationships between the detected cluster centers and the city's amenities, which provides an intuitive explanation of criminal contagion.

Keywords: crime data, Dirichlet process, linear network, Markov chain Monte Carlo, spatio-temporal point processes

1 Introduction

Research in criminology has shown that crime spreads as a contagious disease in local areas (Johnson, 2008; Mohler et al., 2011), with contagion rates varying between different types of crimes (Brantingham et al., 2021a,b). The spread of crime dynamics in urban areas shows complex patterns due to the geographical structure of the city (Brantingham et al., 2009; Dong et al., 2024; Song et al., 2013). Therefore, considering the geographical structure can help us better understand crime dynamics, predict future incidents more accurately, and effectively develop prevention strategies. In this manuscript, we study the space-time locations of crime events in Valencia, Spain, recorded from 2018 to 2019, considering the city's road network structure. By using the exact space-time locations of crime events, we propose a novel spatio-temporal point process model that can understand the clustering patterns of the events.

Point process models have been proposed to understand the clustering behavior of crime events. In this context, spatio-temporal Hawkes process models (Park et al., 2021; Reinhart, 2018; Zhuang and Mateu, 2019) can capture clustering and triggering patterns by modeling the intensity through the past history of the process. Multivariate point processes have also been studied to model different crime types. Hessellund et al. (2022) developed a semiparametric regression model for the intensity function that depends on an unspecified factor common to all crime types. Briz-Redón and Mateu (2023) introduced a mechanistic bivariate spatio-temporal model to study the intensity of two crime types. Mohler (2014) proposed a marked point process model for multiple crime types, which can capture both short-term and long-term hotspots. However, these approaches have limited applicability to our particular data and motivating problem because they do not consider the road network structure. Our crime data can be naturally spatially inhomogeneous due to the network geometry, which additionally poses a significant challenge over classical spatio-temporal point process models. Specifically, if we do not consider the network structure, the places inaccessible to people could also be considered in the analysis. Furthermore, even if the two points are closely located in terms of Euclidean distances, the dis-

tance over the roads can be different depending on the network structure. Without considering such geometric structure, there can be non-negligible biases in the statistical inference.

There is a growing literature on computational methods for point processes on linear networks (see Baddeley et al. (2021) for a comprehensive review). Kernel density estimation methods have already been developed, such as the heat kernel (McSwiggan et al., 2017) that uses the density of a Brownian motion on the network. Rakshit et al. (2019b) proposed a convolution kernel estimator using a fast Fourier transformation. Moradi and Mateu (2020) developed summary statistics for point processes on a linear network, including the K-function and pair correlation function. D’Angelo et al. (2023) studied the local version of inhomogeneous second-order statistics for spatio-temporal point processes. Rakshit et al. (2019a) developed a memory-efficient algorithm to compute second-order summary functions of point patterns on a linear network. Recently, in a more complex scenario where marks are attached to each event, Matthias et al. (2024) and Matthias and Moradi (2024) have developed summary statistics for various mark types, including functional marks.

Although these previous works are useful for exploratory analysis, they do not employ model-based approaches. Developing point process models on road networks still remains challenging due to computational and inferential complexities. Recently, several spatio-temporal point process models have been studied in the context of linear networks. D’Angelo et al. (2022) proposed Gibbs point processes and log-Gaussian Cox processes to study the patterns of visitor stops by touristic attractions. D’Angelo et al. (2024) also developed spatio-temporal Hawkes point process models by including the network geometry in the inference procedure. They show that the proposed model fits much better compared to the planar one (Zhuang and Mateu, 2019). Gilardi et al. (2024) developed a non-separable intensity function to model ambulance interventions on road networks. Apart from these contributions, no further model-based strategies have been proposed.

Although these approaches can describe spatio-temporal patterns of the process defined over linear networks, it is not trivial to detect the space-time clustering structure of crime events. Furthermore, fully Bayesian approaches have been under-explored. Such methods offer a natural framework for quantifying uncertainties within complex hierarchical models.

In this line, we propose a spatio-temporal Dirichlet process (DP) mixture model to analyze crime events that occurred in the road network of the city. DP mixture models have been widely

developed in many disciplines, for instance, to study crime patterns (Taddy, 2010), clustering population genetics data (Reich and Bondell, 2011), and to detect disease hotspots (Park et al., 2023). We indeed use a DP prior in our Bayesian hierarchical model to automatically choose the number and location of cluster centers of crime events. To account for the structure of the linear network in the city, we adopt the convolution kernel estimator (Rakshit et al., 2019b), which can be quickly computed using the fast Fourier transformation.

The outline of the remainder of this paper is as follows. In Section 2, we describe the crime events data in Valencia, Spain. We also provide an exploratory data analysis for the dataset. In Section 3, we propose a spatio-temporal DP mixture model on a linear network and describe details about model inference. In Section 4, we apply our method to real crime data, illustrating that our model can capture the spatio-temporal cluster centers of crime events. In addition, we study the relationship between cluster centers and the amenities of the city, which provides important sociological interpretations. In Section 5, we conclude the paper with a summary and some further discussion.

2 Data description and exploratory analysis

The dynamics of crime contagion are particularly complex within urban settings, influenced heavily by the geographic layout of the city. While crimes occur in a continuous space (*e.g.*, within a city area measured by longitude and latitude), they are mostly confined to the street networks, influencing both the escape routes of criminals and the spatial distribution of crime. Early research also suggests that crime’s contagious effects propagate along these street networks instead of dispersing freely, as evidenced by a fitted non-parametric influence kernel from real crime events. Motivated by these facts, in this section, we describe our crime data and provide some first exploratory data analysis.

2.1 Data: crime events in Valencia, Spain

Valencia is a city on the Mediterranean coastline that has a population of more than 1.5 million (Dong et al., 2024). The crime data in this study is collected by the local police department in Valencia (Spain) and records the exact location and time for each crime event, allowing us to

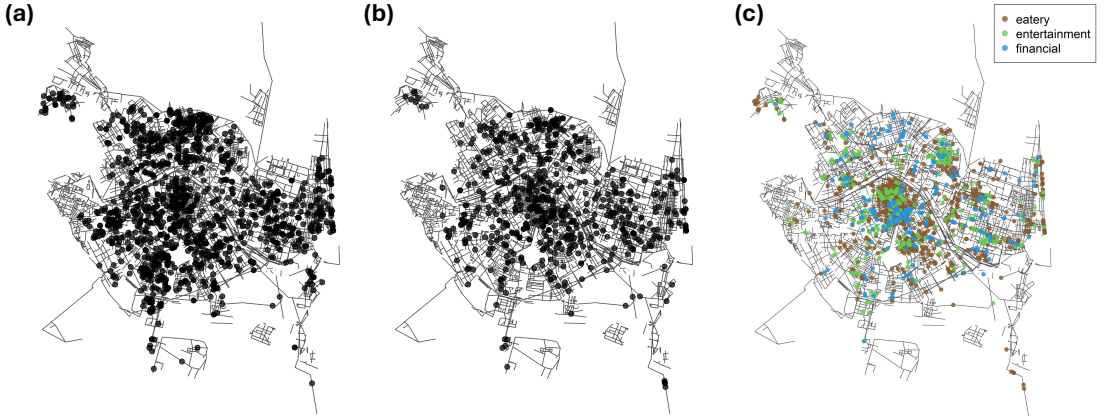


Figure 1: Locations of (a) robbery incidences, (b) theft incidences, and (c) amenities.

use the framework of spatio-temporal point processes. The recorded events are categorized into two distinct types, including: (a) *Robbery* (referring to thefts involving physical assault), and (b) *Theft* (referring to thefts executed smoothly without the use of force). Figure 1a and 1b depicts the locations of these two crimes in the city. In our analysis, we used observations within 500 meters of each single street and projected them on the closest street, resulting in 1,423 records of robbery and 695 records of theft from 2018-01-01 to 2019-12-31 in the city of Valencia (Spain). We describe further details of the street network in Section 2.2. We observe that the spatial patterns of both crimes are quite similar, occurring mainly towards downtown rather than in the outskirts of the city, with lots of variations in both the degree of the vertices and the lengths of the streets.

In addition to crime events, to investigate the relationship between the patterns of the reported crimes and the surrounding urban environment, we also have the geographical locations of different amenities in Valencia, including ATMs, banks, bars, cafes, marketplaces, nightclubs, police stations, pubs, and restaurants. In our study, we categorize the amenities into three groups: (a) entertainment (bars, nightclubs, pubs, with 286 amenities), (b) financial (ATMs, banks, with 246 amenities), and (c) eatery (cafes, restaurants, with 940 amenities). Figure 1c illustrates the locations of these amenities in the city.

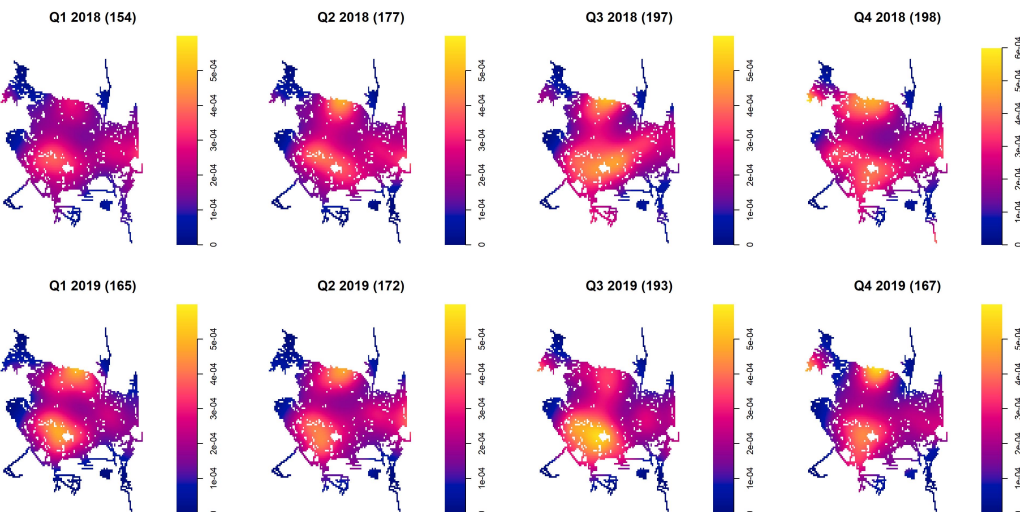
2.2 Exploratory data analysis

Here, we set some background for point patterns on networks while providing some motivation for a DP mixture model. Consider a linear network $\mathcal{L} = \bigcup_{i=1}^n l_i \subseteq \mathbb{R}^2$, as a finite union of line segments $l_i \subseteq \mathbb{R}^2$ (Baddeley et al., 2021). The line segments are defined as $l_i = [u_i, v_i] = \{ku_i + (1-k)v_i : 0 \leq k \leq 1\}$, where $u_i, v_i \in \mathbb{R}^2$ are the endpoints of l_i . For $i \neq j$, the intersection of l_i and l_j is empty or an endpoint of both segments. When considering a time domain $\mathcal{T} \subseteq \mathbb{R}^+$, we can introduce a spatio-temporal point process \mathbf{X} over the bounded domain $\mathcal{L} \times \mathcal{T}$. This process thus contains information about the space-time locations for the crime events.

We first convert Valencia’s street network as a spatial object using `osmdata` (Mark Padgham et al., 2017) package in `R`. We can then represent the data through a projected coordinate reference system (EPSG code: 2062) of Spain that measures units in meters. Specifically, we select all the road features inside a rectangular window (with width 10.95km and height 13.73km) defined by spatial coordinates, including Valencia border. Then, we convert the data into a linear network format (i.e., `linnet` object in `spatstat.linnet` package). The linear network of Valencia contains 69,596 vertices (nodes) and 51,556 line segments (edges). However, using all line segments in the analysis is impractical because street crime events may not occur on specific road types (*e.g.*, highways). Furthermore, it is computationally infeasible to consider the entire road network due to memory issues. Therefore, we chose such streets where crime events could potentially occur, including residential streets, living streets, pedestrian streets, footways, steps, corridors, sidewalks, crossings, and cycleways. Residential streets serve as access to housing. Living streets are residential areas where pedestrians are legally prioritized, and vehicle speeds are strictly restricted. Footways are designated pathways primarily intended for pedestrian use. Corridors are hallways within buildings. Furthermore, we exclude the region where crime events are not observed. Following this procedure, we finally obtained a linear network consisting of 8,392 vertices (nodes) and 6,972 line segments (edges), referring to Valencia, whose total length of all line segments is approximately 805.94km.

To understand the pattern of both types of crime events, we first compute first-order spatial intensities (depicted in Figure 2) by using the convolution kernel estimator (Rakshit et al., 2019b) that accounts for the street structure. We use Scott’s rule (Scott, 2015) to select the bandwidth

(a)



(b)

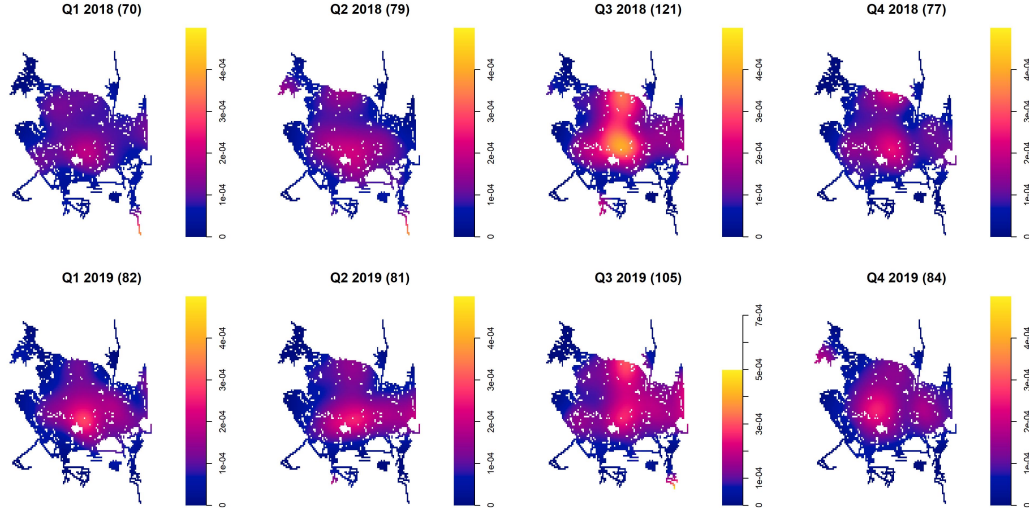


Figure 2: Estimated first-order spatial intensity of (a) robbery and (b) theft by quarters and corresponding crime counts in the parentheses.

for kernel density estimation. Figure 2 illustrates that robbery crime events show higher intensity values in the top and bottom areas of the city, while theft crime events are more concentrated in the center of the city. These findings are aligned with Figure 1.

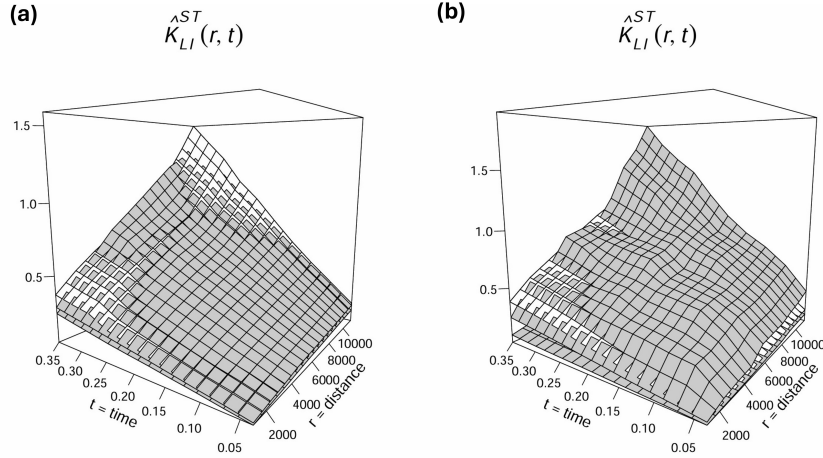


Figure 3: Estimated K -function for (a) robbery and (b) theft. Gray colors are simulation envelopes generated from homogenous Poisson processes, with the lower surface representing the minimum and the upper one representing the maximum K -functions. White colors indicate K -functions from the observed crime data.

We compute the linear network K -function (Moradi and Mateu, 2020) to study second-order characteristics of the point patterns. Specifically, the K -function is defined as

$$K_{LI}^{ST}(r, t) = \mathbb{E} \left[\sum_{(\mathbf{x}, t_x) \in X} \frac{\mathbb{1}\{0 < d_{\mathcal{L}}(\mathbf{u}, \mathbf{x}) < r, |t_u - t_x| < t\}}{\lambda(\mathbf{x}, t_x) M((\mathbf{u}, t_u), d_{\mathcal{L}}(\mathbf{u}, \mathbf{x}), |t_u - t_x|)} |(\mathbf{u}, t_u) \in X \right], \quad (1)$$

where $\lambda(\mathbf{x}, t_x)$ is the first-order intensity and $M((\mathbf{u}, t_u), r, t)$ is the number of points lying exactly at the shortest-path distance r and the time distance t away from (\mathbf{u}, t_u) . In (1), $d_{\mathcal{L}}(\mathbf{u}, \mathbf{x})$ is shortest distance between \mathbf{u} and \mathbf{x} and $|\cdot|$ is the Euclidean distance. Following Moradi and Mateu (2020), we obtain a nonparametric estimate of the K -function, $\hat{K}_{LI}^{ST}(r, t)$. Figure 3 shows that the observed K -functions exceed simulation envelopes, indicating that crime events (both robbery and theft) show a clustering behavior on certain space-time distances. Following Moradi and Mateu (2020), we also compute a p-value to test the null hypothesis of Poissonness (absence

of any sort of clustering), defined as

$$T = \int \int \frac{\hat{K}_{LI}^{ST}(r, t) - E_K(r, t)}{\sqrt{V_K(r, t)}} dr dt,$$

$$\text{p-value} = \frac{1 + \sum_{i=1}^m \mathbb{1}\{T_i > T^*\}}{m + 1}, \quad (2)$$

where E_K and V_K are the mean and variance of $\hat{K}_{LI}^{ST}(r, t)$. In (2), each T_i is computed from a simulated point pattern generated from a homogeneous Poisson process (i.e., null hypothesis), and T^* is computed from the observed point pattern. The p-values for robbery and theft were 0.02 and 0.04, respectively; therefore, we can conclude that the crime events are not compatible with a homogeneous spatio-temporal Poisson process and, indeed, highlight structures with varying clustering degrees.

3 A Dirichlet process mixture model on a linear network

We propose and develop a spatio-temporal DP mixture model considering the geometrical structure of the linear network. The method can detect unobserved cluster centers of street crimes and underpin hotspots.

3.1 Model framework

Let $\{(\mathbf{x}_i, t_i)\}_{i=1}^N$ be a realization of the point process \mathbf{X} over the bounded domain $\mathcal{L} \times \mathcal{T}$. We consider the space domain over the linear network $\mathcal{L} \in \mathbb{R}^2$, and a normalized time domain $\mathcal{T} = [0, 1]$. In our problem, each (\mathbf{x}_i, t_i) denotes the location and time of a crime event. We introduce the latent space-time cluster centers as $\mathbf{c} = \{(\mathbf{c}_j^s, c_j^t)\}_{j=1}^M \in \mathcal{L} \times \mathcal{T}$. To assign an i th observation to a cluster, we define the cluster membership variable $g_i \in \{1, \dots, M\}$ and model the membership variable as a DP prior (Ishwaran and James, 2001). Specifically, we model a g_i as

$$g_i \sim \text{Categorical}(q_1, \dots, q_M),$$

where q_1, \dots, q_M represents the cluster probabilities for crime events. Then we model the cluster membership probabilities as the stick-breaking process prior (Sethuraman, 1994):

$$q_j = \begin{cases} U_1, & \text{for } j = 1 \\ U_j \prod_{m=1}^{j-1} (1 - U_m), & \text{for } j = 2, \dots, M, \end{cases} \quad (3)$$

where $U_1, \dots, U_m \stackrel{\text{iid}}{\sim} \text{Beta}(1, b_u)$ with rate parameter b_u . In our analysis, we set a hyperprior for b_u as $\text{Gamma}(1, 1)$ and $\text{Gamma}(1, 1/4)$, following Reich and Bondell (2011). In the stick-breaking process prior, the initial mixture probability q_1 is represented as a beta random variable U_1 . For $j = 2, \dots, M$, the subsequent mixture probabilities q_j are obtained by multiplying $1 - \sum_{m=1}^{j-1} q_m$, the remaining probability, with U_j , the proportion assigned to the j th cluster component. Theoretically, (3) considers an infinite number of clusters. However, in practice, we approximate it with a sufficiently large $M < \infty$. The remaining probabilities $1 - \sum_{m=1}^{j-1} q_m$ become 0 for large j ; therefore, no observation is assigned to the j th cluster. From this finite representation, we can automatically choose the number of non-empty cluster centers.

After we assign the cluster membership to each observation, we model the space-time locations of crime events. Specifically, we define the conditional distribution for a given g_i as

$$f((\mathbf{x}_i, t_i) | g_i = j) \propto K_S(\mathbf{x}_i; \mathbf{c}_j^s, w_s) K_T(t_i; c_j^t, w_t), \quad (4)$$

where $K_S(\cdot)$ and $K_T(\cdot)$ are spatial and temporal kernels, respectively. In our study, we use $K_T(t_i; c_j^t, w_t)$ as a Gaussian kernel with center c_j^t and a standard deviation w_t (temporal range of cluster centers). There are several options for the spatial kernel $K_S(\cdot)$ that can account for the network geometry (see Baddeley et al. (2021) for a comprehensive review). One might consider the equal-split continuous kernel estimator (Okabe and Sugihara, 2012), which is a path enumeration method. At each fork in the linear network, the method divides the remaining tail mass at the vertex equally across the outgoing line segments. Therefore, the method can preserve the total mass. However, the implementation of the equal-split continuous kernel estimate is computationally demanding for large observations with complex street structures, as happens

in our case. The heat kernel (McSwiggan et al., 2017), which exploits the connection between kernel smoothing and diffusion, can be another option. However, we observe that the heat kernel is not appropriate for our application because the computation time increases quadratically with increasing bandwidth. For practical implementation, we use the convolution kernel estimator (Rakshit et al., 2019b). This convolution kernel estimator of the intensity with uniform correction is given by

$$K_S(\mathbf{x}_i; \mathbf{c}_j^s, w_s) = \frac{\kappa(\mathbf{x}_i; \mathbf{c}_j^s, w_s)}{c_{\mathcal{L}}(\mathbf{c}_j^s)}, \quad (5)$$

where $c_{\mathcal{L}}(\mathbf{c}_j^s) = \int_{\mathcal{L}} \kappa(\mathbf{v}; \mathbf{c}_j^s, w_s) d_1 \mathbf{v}$ is a correction term, and \mathbf{v} is an arbitrary point on \mathcal{L} . In (5), the numerator κ is a planar Gaussian kernel with a smoothing bandwidth w_s . Note that we can interpret it as a spatial range of clusters since the bandwidth is equivalent to the standard deviation of the Gaussian kernel (Chiu, 1991). The denominator in (5) is a convolution of the kernel $\kappa(\cdot)$ with the arc-length measure on the network, and thus the kernel $K_S(\cdot)$ can account for the geometrical structure of the street network. In particular, the correction term $c_{\mathcal{L}}(\mathbf{c}_j^s)$ can be obtained through Monte Carlo integration

$$c_{\mathcal{L}}(\mathbf{c}_j^s) \approx \frac{|\mathcal{L}|}{N} \sum_{k=1}^N \kappa(\mathbf{v}_k; \mathbf{c}_j^s, w_s), \quad (6)$$

where $\mathbf{v}_1, \dots, \mathbf{v}_N$ are generated from \mathcal{L} , which is a uniform distribution over the linear network.

In our case, we observe that $N = 1,000$ can provide an accurate Monte Carlo approximation.

We thus model the membership variable $g_i \sim \text{Categorical}(\tilde{q}_{i1}, \dots, \tilde{q}_{iM})$, where each \tilde{q}_{ij} is set as

$$\tilde{q}_{ij} \propto q_j K_S(\mathbf{x}_i; \mathbf{c}_j^s, w_s) K_T(t_i; c_j^t, w_t), \quad j = 1, \dots, M. \quad (7)$$

Equation (7) implies that the i th observation is assigned to the j th cluster if (\mathbf{x}_i, t_i) is close to (\mathbf{c}_j^s, c_j^t) . In (3), we assign the stick-breaking prior for q_j , and this ensures only $M^* (< M)$ non-empty clusters. From the mixture model specified above, the full likelihood

function is of the form

$$L(\boldsymbol{\theta} | \mathbf{X}, \mathbf{c}) \propto \prod_{i=1}^N \left[\sum_{\forall j \text{non-empty}} q_j K_S(\mathbf{x}_i; \mathbf{c}_j^s, w_s) K_T(t_i; c_j^t, w_t) \right], \quad (8)$$

where $\boldsymbol{\theta} = (w_s, w_t)$ is a model parameter. With a prior specification, the joint posterior distribution can be formulated as $\pi(\boldsymbol{\theta}, \mathbf{c}, \{g_i\}_{i=1}^N, \{U_j\}_{j=1}^M, b_u | \mathbf{X})$. We use uniform priors on w_s, w_t . Since the average length of each street in Valencia is around $115.597m$ and points over $2km$ apart are considered distant for clustering, we set the lower and upper bounds for w_s as 100 and 1,000 metres, respectively. Here, we also consider the criminological literature, which widely uses a $150m \times 150m$ grid as a spatial unit (Block, 2000; Santitissadeekorn et al., 2018). This unit size reflects the largest area a single police officer typically covers on foot patrol within a designated beat (Zhang et al., 2022). For w_t , we set the lower bound of the prior as 0. For \mathbf{c} , we use the uniform prior defined over the network and the time period. To accelerate computation, we discretize the network domain \mathcal{L} through 50×50 pixels Δ . Then, we propose a spatial location of the cluster center from the discretized uniform prior. The hierarchical model structure and full conditionals for all components are described in the supplementary material. Algorithm 1 summarizes the Markov chain Monte Carlo (MCMC) procedure for Bayesian inference.

3.2 Post-Processing

Post-processing is required to obtain the final results from DP-based methods due to the label switching issue (see, *e.g.*, Medvedovic and Sivaganesan, 2002; Dahl, 2006; Reich and Bondell, 2011), where labels for any two different clusters can be swapping at a certain point of the MCMC chain. Without post-processing, each cluster label may represent multiple clusters in the data, leading to spurious multi-modality and overestimated variability. To address this, we identify the b^* th iteration of the MCMC chain that minimizes a loss related to cluster memberships, as follows:

$$b^* = \arg \min_b \left\{ \sum_{i=1}^N \sum_{j=1}^N \{ \mathbb{1}(g_i^b = g_j^b) - d_{ij} \}^2 \right\}, \quad d_{ij} = \sum_{b=1}^B \{ \mathbb{1}(g_i^b = g_j^b) / B \}$$

Here, B denotes the total number of iterations in the MCMC, and g_i^b denotes the membership of the sampled segment for the i th observation in the b th iteration. This solution minimizes

Algorithm 1 MCMC algorithm for an STDP on a linear network

Given $\{\boldsymbol{\theta}^{(b)}, \mathbf{c}^{(b)}, \{g_i^{(b)}\}_{i=1}^N, \{U_j^{(b)}\}_{j=1}^M, b_u^{(b)}\}$ at the b -th iteration

Update the model parameters $\boldsymbol{\theta}^{(b+1)}$:

Propose $\boldsymbol{\theta}^* \sim q(\cdot | \boldsymbol{\theta}^{(b)})$ and accept $\boldsymbol{\theta}^{(b+1)} = \boldsymbol{\theta}^*$ with probability

$$\alpha = \min \left\{ 1, \frac{\pi \left(\boldsymbol{\theta}^* | \mathbf{c}^{(b)}, \{g_i^{(b)}\}_{i=1}^N, \{U_j^{(b)}\}_{j=1}^M, b_u^{(b)} \right)}{\pi \left(\boldsymbol{\theta}^{(b)} | \mathbf{c}^{(b)}, \{g_i^{(b)}\}_{i=1}^N, \{U_j^{(b)}\}_{j=1}^M, b_u^{(b)} \right)} \right\}$$

Update cluster index probability for each observation:

Generate $g_i^{(b+1)} \sim \text{Categorical}(\tilde{q}_{i1}, \dots, \tilde{q}_{iM})$, where

$$\tilde{q}_{ij} \propto q_j K_S(\mathbf{x}_i; \mathbf{c}_j^s, w_s) K_T(t_i; c_j^t, w_t)$$

for $i = 1, \dots, N$ and $j = 1, \dots, M$.

Update Dirichlet process parameters:

Generate

$$U_j^{(b+1)} \sim \text{Beta}\left(1 + \sum_{i=1}^N \mathbb{1}\{g_i^{(b+1)} = j\}, b_u^{(b)} + \sum_{i=1}^N \mathbb{1}\{g_i^{(b+1)} > j\}\right)$$

for $j = 1, \dots, M$.

Generate

$$b_u^{(t+1)} \sim \text{Gamma}\left(M, c - \sum_{j=1}^{M-1} \log(1 - U_j^{(t+1)})\right)$$

Update space-time cluster centers $\mathbf{c}^{(b+1)}$:

Propose $(\mathbf{c}_j^{s*}, c_j^{t*}) \sim \frac{1}{|\Delta| \mathcal{T}}$ and accept $(\mathbf{c}_j^{s(b+1)}, c_j^{t(b+1)}) = (\mathbf{c}_j^{s*}, c_j^{t*})$ with probability

$$\alpha = \min \left\{ 1, \frac{\pi \left((\mathbf{c}_j^{s*}, c_j^{t*}) | \boldsymbol{\theta}^{(b+1)}, \{g_i^{(b+1)}\}_{i=1}^N, \{U_j^{(b+1)}\}_{j=1}^M, b_u^{(b+1)} \right)}{\pi \left((\mathbf{c}_j^{s(b)}, c_j^{t(b)}) | \boldsymbol{\theta}^{(b+1)}, \{g_i^{(b+1)}\}_{i=1}^N, \{U_j^{(b+1)}\}_{j=1}^M, b_u^{(b+1)} \right)} \right\}$$

for $j = 1, \dots, M$.

the posterior expected loss for estimated segment membership proposed by Binder (1978) in Bayesian model-based clustering (Dahl, 2006).

3.3 Model assessment

We evaluate the performance of our model by comparing the empirical proportion of data points with the theoretical proportion derived from the likelihood function. Consider the rectangular cubes covering our spatio-temporal domain. The theoretical proportion corresponding to the cube $[\alpha_g, \beta_g]^3$ is calculated as

$$p_g^t = \int_{[\alpha_g, \beta_g]^3 \in \mathcal{L} \times \mathcal{T}} \sum_{\forall j \text{ non-empty}} q_j K_S(\mathbf{x}; \mathbf{c}_j^s, w_s) K_T(t; c_j^t, w_t) d\mathbf{X},$$

where $\mathbf{X} \in \mathcal{L} \times \mathcal{T}$ represents the spatio-temporal point process. Since the integral in the above equation is analytically intractable, we compute an approximation, \hat{p}_g^t , through numerical integration. This is implemented with the `pmvnorm` function from the R package `mvtnorm`. Similarly, we compute the observed proportion of data points corresponding to the cube $[\alpha_g, \beta_g]^3$ as

$$p_g^o = \frac{\text{the number of observations in } [\alpha_g, \beta_g]^3}{\text{total number of observations}}.$$

We compare \hat{p}_g^t and p_g^o computed on each cube. Note that if we use too small cubes, we would have a lot of zeros for p_g^o because there will be no observation in $[\alpha_g, \beta_g]^3$. On the other hand, if we use too large cubes, the approximation error for \hat{p}_g^t becomes larger because the cubes will also cover the region without the roads. To address this, we first construct $G_s = 200 \times 200 \times 10$ number of subgrid points (i.e., high-resolution grid) over $\mathcal{L} \times \mathcal{T}$ and compute \hat{p}_g^t and p_g^o at each cube. Then, we aggregate them into larger, nonoverlapping grid points $G = 5 \times 5 \times 10$ that also cover $\mathcal{L} \times \mathcal{T}$. We provide details on grid computation in the supplementary material.

4 Application

We applied our proposed method to the Valencia crime data described in Section 2.1. The code was implemented in R version 4.1.3 (R Core Team, 2022) and executed on an AMD Ryzen 9

5950X 16-core processor. The complete MCMC analysis, comprising 20,000 iterations and post-processing, required approximately 54.23 hours for crime type robbery, and 29.78 hours for crime type theft. The maximum number of clusters was set to 80 for robbery and 70 for theft, with the number of detected clusters automatically determined to be below these limits. Here, note that we need to penalize the maximum number of cluster centers. Setting the maximum number of clusters excessively high with small range parameters results in dense centers throughout the region, leading to overfitting. However, if there are few centers, it may not detect centers in the area.

4.1 Crime hotspots

Figure 4 shows detected cluster centers and their offspring for each crime type, analyzed quarterly over the two-year period. Robbery cluster centers were more frequently detected in Q2 of 2018 and Q3 of 2019, while theft clusters were more commonly detected in Q3 of 2018. These findings align with prior research on seasonal variations in crime levels (Cohn, 1990; Farrell and Pease, 1994; McDowall et al., 2011). Numerous studies have demonstrated that both violent and property and personal crimes tend to peak during the summer or fall months (Deckard and Schnell, 2023; Haberman et al., 2018; Hipp et al., 2004; Kim and Wo, 2022). This pattern is likely attributable to shifts in individuals' routine activities, such as vacation and outdoor events, which increase the likelihood of convergence between potential offenders and suitable victims in the absence of effective guardianship (Cohen and Felson, 1979). Additional evidence supporting this argument is the peak in tourist numbers in Valencia between May and October (Q2 and Q3) in both 2018 and 2019 (Instituto Nacional de Estadística, 2025).

Figure 5 represents the posterior mean of the density on the linear network, calculated by our model (8), with the estimated range parameter plugged in. This figure shows robbery highlighted in yellow in the upper area in Q2 of 2018 and in the bottom area in Q3 of 2019. For theft, the number of detected cluster centers is smaller than that for robbery, with a denser concentration in Q3 of 2018. Interestingly, the patterns of robbery and theft exhibit similarities in Q3 of 2018. For both crime types, hotspots appear to be shifting from one quarter to the next. This observation supports the literature indicating that hotspots exhibit short-term stability, typically lasting only

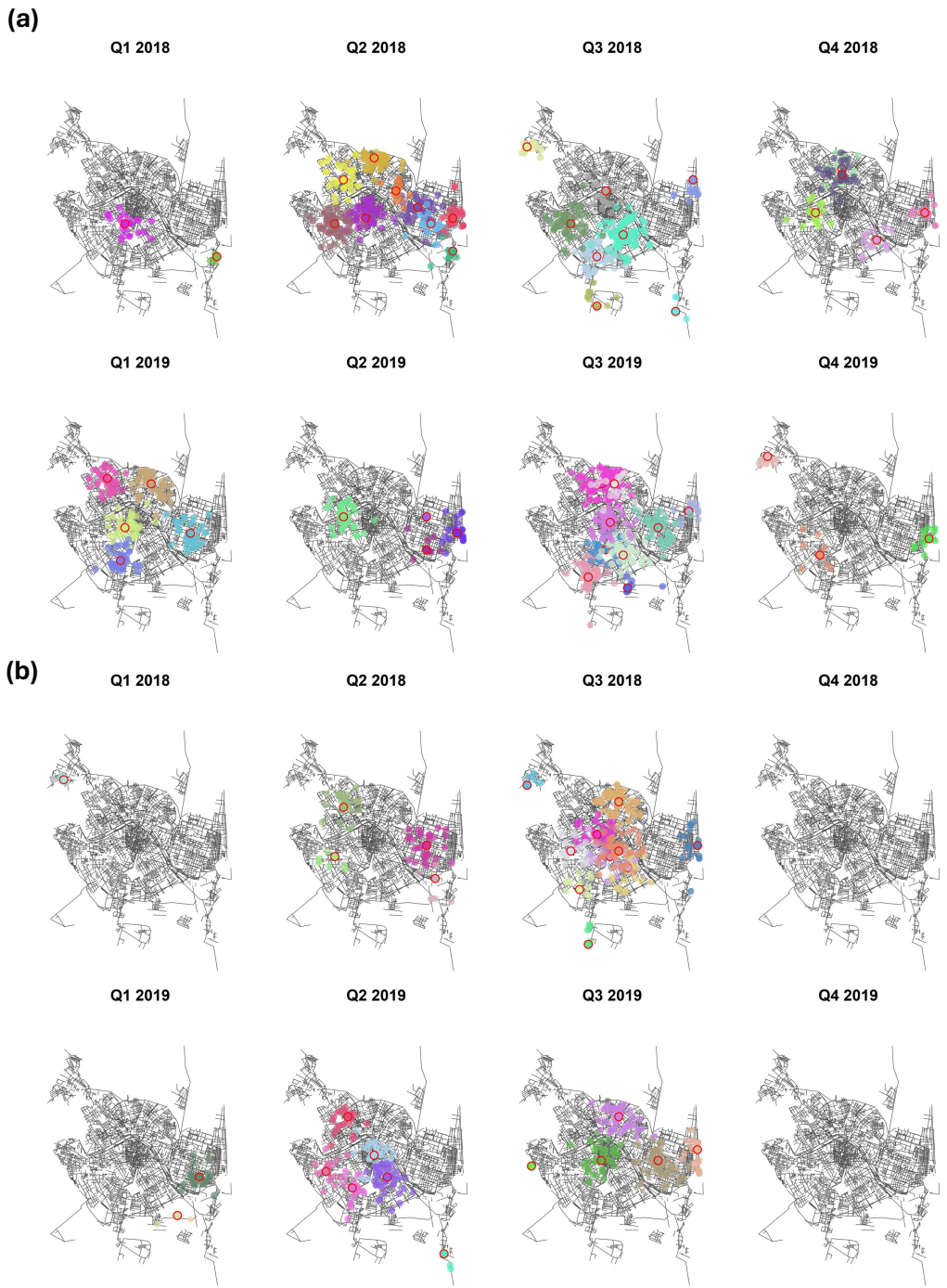


Figure 4: Detected cluster centers and their offspring by quarters of (a) robbery and (b) theft. The red-outlined dots indicate detected cluster centers, while the surrounding dots of the same color represent their offspring belonging to the same cluster.

a few months (Deckard and Schnell, 2023; Groff et al., 2015). Consequently, focusing police and social service resources in crime hotspots for brief periods may be effective in achieving notable reductions in crime (Weisburd, 2018).

Figure 6a shows scatter plots of the estimated and observed proportions, \hat{p}_g^t and p_g^o . The points are scattered around the straight one-to-one line for both crime types, indicating that our model effectively captures the spatio-temporal densities of points on a linear network.

We fitted the model given by Equation (8) to the data described in Section 2 using Algorithm 1. The estimated parameters are summarized in Table 1. For robbery, the space and time range parameters are about $545m$ and 0.14 (roughly 3 months and 11 days) respectively, indicating that 95% of observed points lie within approximately circles of $2 \times 545m$ and temporal intervals of 6 months and 22 days. For theft, the space and time range parameters are about $563m$ and 0.142 (roughly 3 months and 12 days). Accordingly, 95% of observed points fall within circles of $2 \times 563m$ and within temporal intervals of 6 months and 24 days. With this information at hand, we can delineate the spatio-temporal structure and behavior of our crime data. These estimates align with the observation that both types of crime exhibit temporal concentration in two seasonal quarters—Q2 and Q3, which correspond to the summer and fall months. Additionally, the findings suggest that the spatial diameter of each crime cluster is approximately 1.1 kilometers, with theft clusters being slightly more dispersed than robbery clusters.

	w_s (space)	w_t (time)
Robbery	544.798 (511.308, 572.985)	0.140 (0.131, 0.150)
Theft	563.402 (536.571, 587.816)	0.142 (0.131, 0.155)

Table 1: Posterior means and 95% HPD intervals (parenthesis) of space and time range parameters for robbery and theft.

4.2 Association of amenities with crimes

Figure 7 illustrates the relative proportions of amenities located within the $2 \times$ (spatial range) from each cluster center. To prevent bias, the weight is calculated as the ratio of the total number of amenities to the count of a specific amenity within the buffer, and the final value is calculated by multiplying this ratio by the specific amenity count. The spatial closeness of amenities to cluster

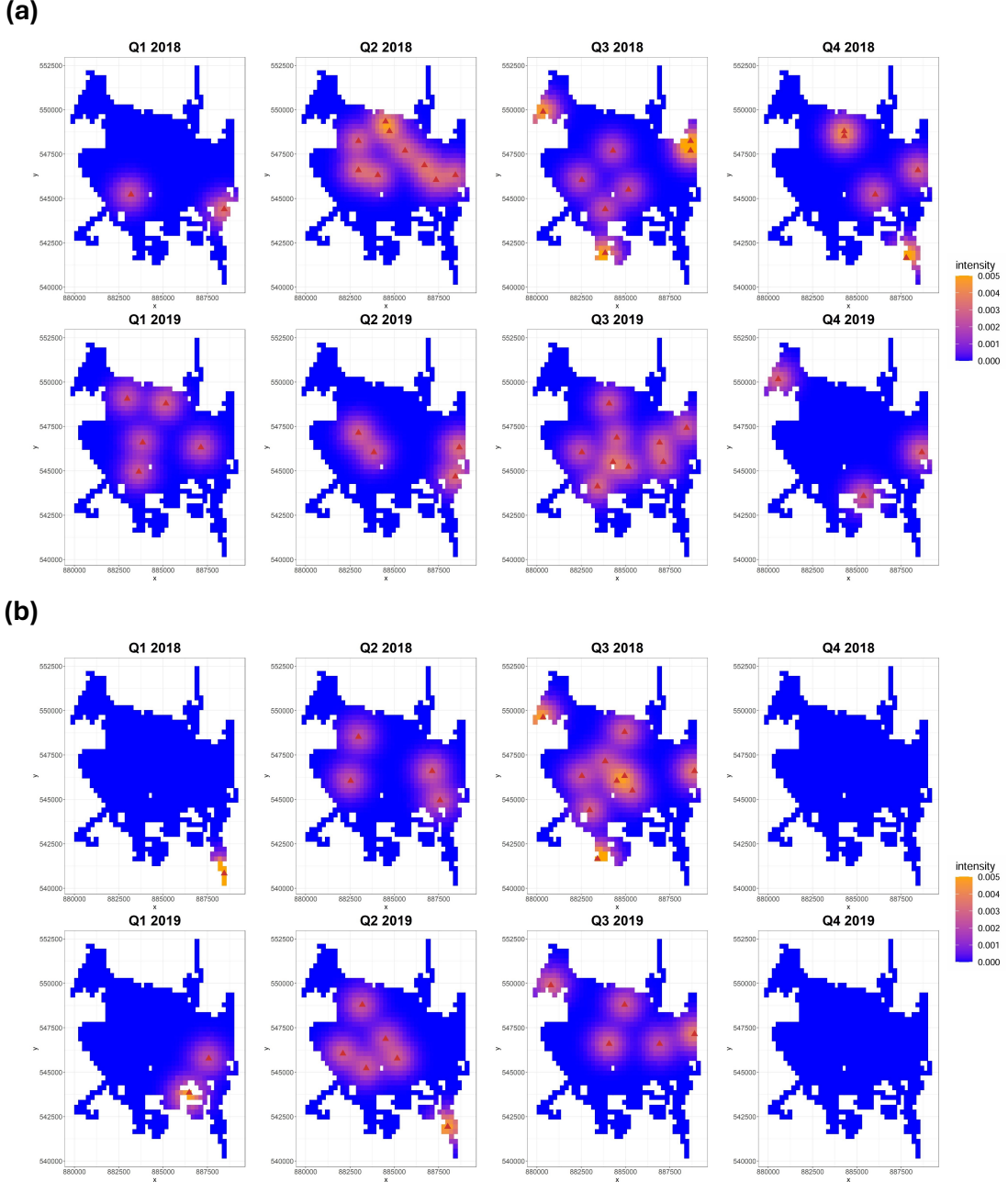


Figure 5: Posterior means of the density of the observed cases of (a) robbery and (b) theft by quarter. Red triangles indicate the detected cluster centers during each period.

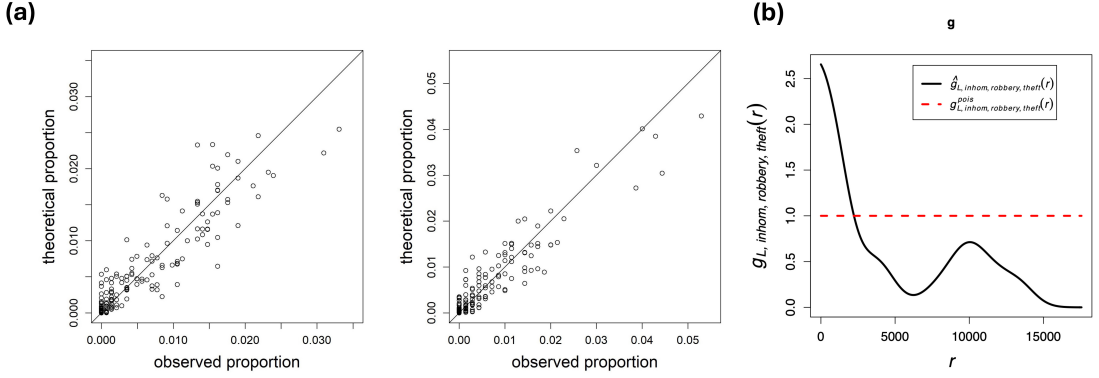


Figure 6: (a): Scatter plots of observed proportion and theoretical proportion (Left: robbery, Right: theft), (b): Multitype pair correlation function. The black solid line represents the inhomogeneous estimate of the pair correlation function and the red dashed line represents 1, the uniform Poisson process.

centers suggests their potential association with the occurrence of crime events. The proportion of amenity types varies across clusters, and a high proportion of a specific amenity type indicates that these amenities are more influential in the cluster. Overall, the distribution of amenities is uneven, with city center exhibiting a higher concentration of financial and entertainment facilities, whereas the outskirts predominantly feature eateries and some financial services (see again Figure 7).

Clusters situated in the bottom-right quadrant, a coastal area, indicate that both crime categories are exclusively influenced by eateries. Note that this area of the city sits around the coast and a lake (called *Albufera*) and is full of restaurants and open-air dining places. Thus, our model offers additional evidence that eateries generate opportunities for crime due to high-traffic nature, elevated levels of activity and visibility, and the presence of stored cash (Brantingham and Brantingham, 1995). The bottom central area, corresponding to the downtown district, is characterized by a high concentration of entertainment-related amenities that attract pedestrians for recreational purposes, while the top central area is primarily defined by the presence of financial establishments.

Throughout the study period, entertainment venues and eateries were more prominently represented in crime clusters, compared to financial amenities. These findings align with prior research examining the relationship between land use and crime (for a review, see (Wilcox and

Eck, 2011)). Specifically, commercial land use is associated with higher crime rates, residential land use with lower crime rates, and office and industrial land uses with increased property crime (Boessen and Hipp, 2015; Haberman and Ratcliffe, 2015; Kinney et al., 2008; Lee et al., 2022; Stucky and Ottensmann, 2009). However, this study only examined amenities related to commercial land use, excluding other types of land use.

4.3 Association between the two crime types

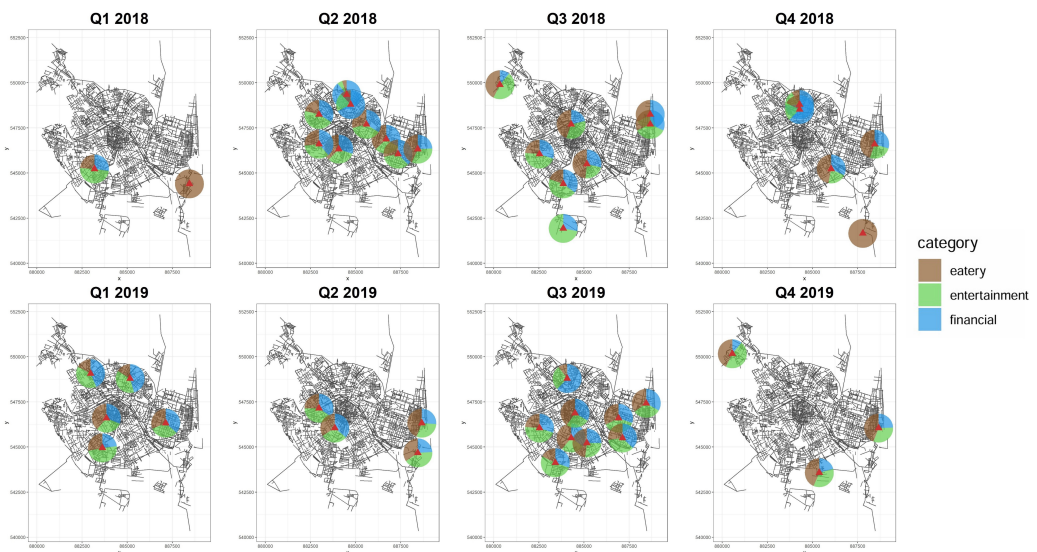
To analyze the association between two crime types, we apply an inhomogeneous multitype pair correlation function on a linear network (Baddeley et al., 2014), which is estimated as

$$\hat{\rho}^{\mathcal{L}, \text{inh}}(r) = \frac{1}{|\mathcal{L}|} \sum_{\mathbf{x}_{1,i} \in \mathbf{X}_1} \sum_{\mathbf{x}_{2,j} \in \mathbf{X}_2} \frac{\kappa(r; d_{\mathcal{L}}(\mathbf{x}_{1,i}, \mathbf{x}_{2,j}), h)}{\hat{\lambda}_1(\mathbf{x}_{1,i}) \hat{\lambda}_2(\mathbf{x}_{2,j}) M(\mathbf{v}, d_{\mathcal{L}}(\mathbf{x}_{1,i}, \mathbf{x}_{2,j}))}, \quad (9)$$

where \mathbf{X}_1 , \mathbf{X}_2 are two spatial point processes on a linear network \mathcal{L} and $\mathbf{x}_{1,i}$, $\mathbf{x}_{2,j}$ are their i th and j th events of any of both types. In (9), $M(\mathbf{v}, d_{\mathcal{L}}(\mathbf{x}_{1,i}, \mathbf{x}_{2,j}))$ is the number of locations $\mathbf{v} \in \mathcal{L}$ that are $d_{\mathcal{L}}(\mathbf{x}_{1,i}, \mathbf{x}_{2,j})$ away from $\mathbf{x}_{1,i}$ (Ang et al., 2012) in terms of the shortest-path distance. $\kappa(r; d_{\mathcal{L}}(\mathbf{x}_{1,i}, \mathbf{x}_{2,j}), h)$ denotes a planar Gaussian kernel centered with the center $d_{\mathcal{L}}(\mathbf{x}_{1,i}, \mathbf{x}_{2,j})$ and the bandwidth h , which is determined using a Scott's rule (Scott, 2015). $\hat{\lambda}_1(\cdot)$, $\hat{\lambda}_2(\cdot)$ stand for the estimated intensity functions of \mathbf{X}_1 and \mathbf{X}_2 .

We computed a multitype pairwise correlation function between spatial cluster centers from the two crime types. From Figure 7, we observe that the centers of the two crimes (red triangles) are close in Q3 of 2018 and Q3 of 2019. Indeed, the pcf plot (see Figure 6b) takes values exceeding 1 at certain spatial distances ($r < 2500$), indicating an attraction tendency. In contrast, we observe that the centers of the two crimes have a repulsive pattern in Q1 of 2019 (Figure 7), and the computed pcf values drop below 1 at around $r > 2500$. These results indicate that robbery and theft crime clusters are more concentrated in the fall when both peak and become more dispersed in other seasons with lower crime activity.

(a)



(b)

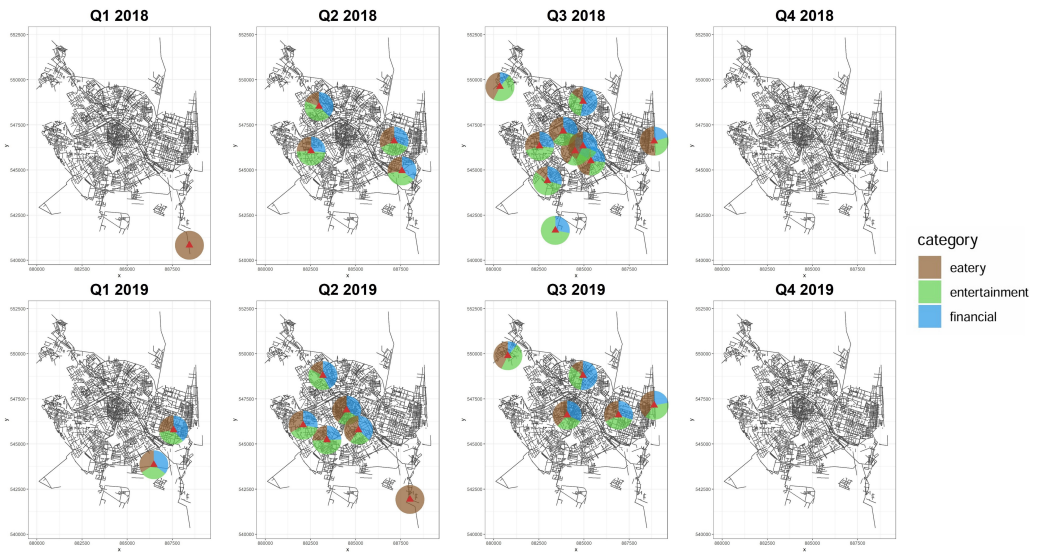


Figure 7: Amenity proportions for each cluster by quarter. Red triangles indicate detected cluster centers. The brown, green, and blue sections show proportions of eatery, entertainment, and financial amenities, respectively. (a) robbery and (b) theft.

5 Discussion

In this paper, we have proposed a Bayesian spatio-temporal point process model on a linear network. With a DP prior, the model can detect unobserved space-time cluster centers of crime incidence over the street network. From the detected cluster centers, we study the association between amenities and crime events, which provides interesting criminological research findings. Furthermore, we have estimated spatio-temporal intensities that can describe the pattern of crime events in the city. We use the computationally efficient convolution kernel estimator (Rakshit et al., 2019b) in our model to account for the geometrical structure of the street network. We have also assessed the performance of the model by comparing the theoretical and empirical densities and observed that our model fits well. To our knowledge, this is the first attempt to consider the Bayesian framework for the point process analysis on a linear network.

There are several caveats to be further considered in future research. In this study, we fitted the model to two crime types separately and analyzed the correlation between their cluster centers. Our model can be extended to a bivariate point process setting. Recently, Briz-Redón and Mateu (2023) proposed a mechanistic bivariate point process over the planar space, assuming that the current crime event is affected by different crime types in the past. Another direction is to model the crime events as a marked point process that has information about the crime type. Several Bayesian approaches have been developed to model data with geographic locations and categorical marks (Jiao et al., 2021; Quick et al., 2015). Incorporating such frameworks into our model would be an interesting extension.

Supplementary Material

Supplementary materials available online contain full conditionals for the MCMC algorithm and grid computation details.

Acknowledgement

This work was supported by the National Research Foundation of Korea (2020R1C1C1A0100386815, RS-2023-00217705) and the IITP (Institute of Information & Communications Technology Plan-

ning & Evaluation)-ICAN (ICT Challenge and Advanced Network of HRD) (IITP-2024-RS-2023-00259934, 10%) grant funded by the Korea government (Ministry of Science and ICT). J. Mateu has been funded by research projects CIAICO/2022/191 from Generalitat Valenciana and PID2022-141555OB-I00 from the Spanish Ministry of Science and Innovation. The authors are grateful to Mehdi Moradi for providing useful sample code and advice.

Data Availability Statement

The datasets and source code can be downloaded from <https://github.com/SujeongLeee/stdplinnet>.

Conflict of Interest Statement

The authors declare that they have no conflicts of interest.

Supplementary material for A Spatio-Temporal Dirichlet Process Mixture Model on Linear Networks for Crime Data

Sujeong Lee, Won Chang, Jorge Mateu, Heejin Lee, and Jaewoo Park

Supplementary Materials for A Spatio-Temporal Dirichlet Process Mixture Model on Linear Networks for Crime Data

Sujeong Lee, Won Chang, Jorge Mateu, Heejin Lee, and Jaewoo Park

A The Bayesian hierarchical model structure

$$\text{Likelihood: } \prod_{i=1}^N \left[\sum_{\forall j \text{ non-empty}} q_j K_S(\mathbf{x}_i; \mathbf{c}_j^s, w_s) K_T(t_i; c_j^t, w_t) \right]$$

Dirichlet process prior: $g_i \sim \text{Categorical}(q_1, \dots, q_M)$

$$q_j = U_1 \text{ for } j = 1 \text{ and } q_j = U_j \prod_{m=1}^{j-1} (1 - U_m) \text{ for } j = 2, \dots, M$$

$$U_1, \dots, U_m \stackrel{\text{iid}}{\sim} \text{Beta}(1, b_u)$$

$$b_u \sim \text{Gamma}(1, c)$$

Parameter prior: $w_s \sim I_{[100, 1000]}(w_s)$

$$w_t \sim I_{[0, \infty)}(w_t)$$

Cluster prior: $\mathbf{c} \sim \frac{1}{|\Delta| \mathcal{T}}$

B Full conditionals for MCMC

1. The conditional distribution of range parameters (w_s, w_t) :

$$\begin{aligned}\pi(w_s, w_t | \text{others}) &\propto \prod_{i=1}^N f((\mathbf{x}_i, t_i) | w_s, w_t) \pi(w_s) \pi(w_t) \\ &\propto \prod_{i=1}^N \left[\sum_{\forall j \text{ non-empty}} q_j K_S(\mathbf{x}_i; \mathbf{c}_j^s, w_s) K_T(t_i; c_j^t, w_t) \right] \times \pi(w_s) \pi(w_t).\end{aligned}$$

2. The conditional distribution of range parameters (w_s, w_t) :

$$\begin{aligned}\pi(w_s, w_t | \text{others}) &\propto \prod_{i=1}^N f((\mathbf{x}_i, t_i) | w_s, w_t) \pi(w_s) \pi(w_t) \\ &\propto \prod_{i=1}^N \left[\sum_{\forall j \text{ non-empty}} q_j K_S(\mathbf{x}_i; \mathbf{c}_j^s, w_s) K_T(t_i; c_j^t, w_t) \right] \times \pi(w_s) \pi(w_t).\end{aligned}$$

3. The conditional distribution of range parameters (w_s, w_t) :

$$\begin{aligned}\pi(w_s, w_t | \text{others}) &\propto \prod_{i=1}^N f((\mathbf{x}_i, t_i) | w_s, w_t) \pi(w_s) \pi(w_t) \\ &\propto \prod_{i=1}^N \left[\sum_{\forall j \text{ non-empty}} q_j K_S(\mathbf{x}_i; \mathbf{c}_j^s, w_s) K_T(t_i; c_j^t, w_t) \right] \times \pi(w_s) \pi(w_t).\end{aligned}$$

4. The conditional distribution of membership variable g_i :

$$\pi(g_i | \text{others}) = \text{Categorical}(\tilde{q}_{i1}, \dots, \tilde{q}_{iM})$$

where

$$\tilde{q}_{ij} \propto q_j K_S(\mathbf{x}_i; \mathbf{c}_j^s, w_s) K_T(t_i; c_j^t, w_t)$$

for $j = 1, \dots, M$.

5. The conditional distribution of space-time cluster centers (\mathbf{c}_j^s, c_j^t) :

$$\pi((\mathbf{c}_j^s, c_j^t) | \text{others}) \propto \prod_{\forall i | g_i=j} q_j K_S(\mathbf{x}_i; \mathbf{c}_j^s, w_s) K_T(t_i; c_j^t, w_t) \times \frac{1}{|\Delta| \mathcal{T}}.$$

for $j = 1, \dots, M$.

6. The conditional distribution of U_j :

$$\pi(U_j | \text{others}) = \text{Beta} \left(1 + \sum_{i=1}^N \mathbb{1}\{g_i = j\}, b_u + \sum_{i=1}^N \mathbb{1}\{g_i > j\} \right).$$

7. The conditional distribution of b_u :

$$\pi(b_u | \text{others}) = \text{Gamma} \left(M - 1 + a, c - \sum_{j=1}^{M-1} \log(1 - U_j) \right),$$

where $a=1$, $c=1$ and $1/4$.

C Grid computation details

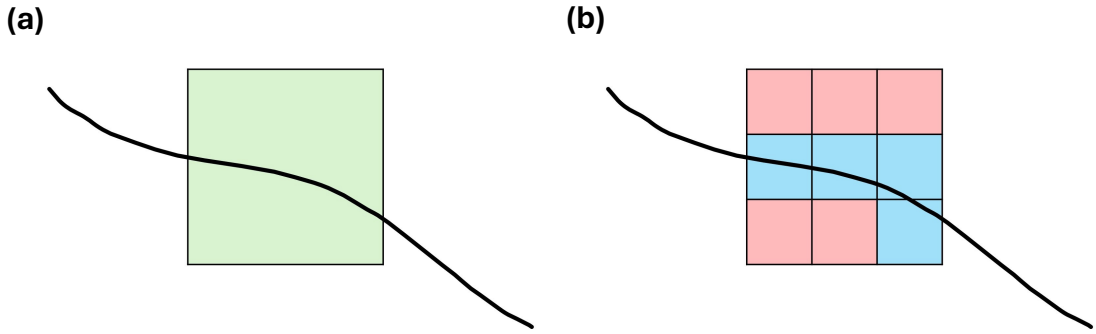


Figure 8: (a) Grid and subgrid (b) covering the road network. Among the cubes belonging to the subgrid, only the part containing the road network (blue colors) was used in the aggregation step.

References

- Ang, Q. W., Baddeley, A., and Nair, G. (2012). Geometrically corrected second order analysis of events on a linear network, with applications to ecology and criminology. *Scandinavian Journal of Statistics*, 39(4):591–617.
- Baddeley, A., Jammalamadaka, A., and Nair, G. (2014). Multitype point process analysis of spines on the dendrite network of a neuron. *Journal of the Royal Statistical Society Series C: Applied Statistics*, 63(5):673–694.
- Baddeley, A., Nair, G., Rakshit, S., McSwiggan, G., and Davies, T. M. (2021). Analysing point patterns on networks—A review. *Spatial Statistics*, 42:100435.
- Binder, D. A. (1978). Bayesian cluster analysis. *Biometrika*, 65(1):31–38.
- Block, R. (2000). Gang activity and overall levels of crime: A new mapping tool for defining areas of gang activity using police records. *Journal of Quantitative Criminology*, 16(3):369–383.
- Boessen, A. and Hipp, J. R. (2015). Close-ups and the scale of ecology: Land uses and the geography of social context and crime. *Criminology*, 53:399–426.

- Brantingham, P. and Brantingham, P. (1995). Criminality of place: Crime generators and crime attractors. *European Journal of Criminal Policy and Research*, 3:5–26.
- Brantingham, P. J., Carter, J., MacDonald, J., Melde, C., and Mohler, G. (2021a). Is the recent surge in violence in american cities due to contagion. *Journal of Criminal Justice*, 76:101848.
- Brantingham, P. J., Yuan, B., and Herz, D. (2021b). Is gang violent crime more contagious than non-gang violent crime. *Journal of Quantitative Criminology*, 37:953–977.
- Brantingham, P. L., Brantingham, P. J., Vajihollahi, M., and Wuschke, K. (2009). Crime analysis at multiple scales of aggregation: A topological approach. In Weisburd, D., Bernasco, W., and Bruinsma, G. J. N., editors, *Putting crime in its place*, chapter 4, pages 87–107. Springer, New York.
- Briz-Redón, Á. and Mateu, J. (2023). A mechanistic bivariate point process model for crime pattern analysis. *Stat*, 12(1):e537.
- Chiu, S.-T. (1991). Bandwidth selection for kernel density estimation. *The Annals of Statistics*, pages 1883–1905.
- Cohen, L. E. and Felson, M. (1979). Social change and crime rate trends: A routine activity approach. *American Sociological Review*, 44:588–608.
- Cohn, E. G. (1990). Weather and crime. *The British Journal of Criminology*, 30:51–64.
- Dahl, D. B. (2006). Model-based clustering for expression data via a dirichlet process mixture model. *Bayesian inference for gene expression and proteomics*, 4:201–218.
- Deckard, M. and Schnell, C. (2023). The temporal (in)stability of violent crime hot spots between months and the modifiable temporal unit problem. *Crime & Delinquency*, 69:1312–1335.
- Dong, Z., Mateu, J., and Xie, Y. (2024). Spatio-temporal-network point processes for modeling crime events with landmarks. *arXiv preprint arXiv:2409.10882*.
- D'Angelo, N., Adelfio, G., Abbruzzo, A., and Mateu, J. (2022). Inhomogeneous spatio-temporal point processes on linear networks for visitors' stops data. *The Annals of Applied Statistics*, 16(2):791–815.

- D'Angelo, N., Adelfio, G., and Mateu, J. (2023). Local inhomogeneous second-order characteristics for spatio-temporal point processes occurring on linear networks. *Statistical Papers*, 64(3):779–805.
- D'Angelo, N., Payares, D., Adelfio, G., and Mateu, J. (2024). Self-exciting point process modelling of crimes on linear networks. *Statistical Modelling*, 24(2):139–168.
- Farrell, G. and Pease, K. (1994). Crime seasonality: Domestic disputes and residential burglary in merseyside 1988-90. *The British Journal of Criminology*, 34:487–498.
- Gilardi, A., Borgoni, R., and Mateu, J. (2024). A nonseparable first-order spatiotemporal intensity for events on linear networks: An application to ambulance interventions. *The Annals of Applied Statistics*, 18(1):529–554.
- Groff, E. R., Ratcliffe, J. H., Sorg, E. T., Joyce, N. M., and Taylor, R. B. (2015). Does what police do at hot spots matter? the philadelphia policing tactics experiment. *Criminology*, 53:23–53.
- Haberman, C. P. and Ratcliffe, J. H. (2015). Testing for temporally differentiated relationships among potentially criminogenic places and census block street robbery counts. *Criminology*, 53:457–483.
- Haberman, C. P., Sorg, E. T., and Ratcliffe, J. H. (2018). The seasons they are a changin': Testing for seasonal effects of potentially criminogenic places on street robbery. *Journal of Research in Crime and Delinquency*, 55:425–459.
- Hessellund, K. B., Xu, G., Guan, Y., and Waagepetersen, R. (2022). Semiparametric multinomial logistic regression for multivariate point pattern data. *Journal of the American Statistical Association*, 117(539):1500–1515.
- Hipp, J. R., Bauer, D. J., Curran, P. J., and Bollen, Kenneth, A. (2004). Crimes of opportunity or crimes of emotion? testing two explanations of seasonal change in crime. *Social Forces*, 82:1333–1372.
- Instituto Nacional de Estadística (2025). Tourist movement on borders, comunitat valenciana, base data.

- Ishwaran, H. and James, L. F. (2001). Gibbs sampling methods for stick-breaking priors. *Journal of the American statistical Association*, 96(453):161–173.
- Jiao, J., Hu, G., and Yan, J. (2021). A bayesian marked spatial point processes model for basketball shot chart. *Journal of Quantitative Analysis in Sports*, 17(2):77–90.
- Johnson, S. D. (2008). Repeat burglary victimisation: a tale of two theories. *Journal of Experimental Criminology*, 4:215–240.
- Kim, Y.-A. and Wo, J. C. (2022). Seasonality and crime in orlando neighbourhoods. *The British Journal of Criminology*, 62:124–144.
- Kinney, J. B., Brantingham, P. L., Wuschke, K., Kirk, M. G., and Brantingham, P. J. (2008). Crime attractors, generators and detractors: Land use and urban crime opportunities. *Built Environment*, 34:62–74.
- Lee, Y.-J., O, S.-H., and Eck, J. E. (2022). Why your bar has crime but not mine: Resolving the land use and crime-risky facility conflict. *Justice Quarterly*, 39:1009–1035.
- Mark Padgham, Bob Rudis, Robin Lovelace, and Maëlle Salmon (2017). osmdata. *Journal of Open Source Software*, 2(14):305.
- Matthias, E., Mateu, J., and Moradi, M. (2024). Function-valued marked spatial point processes on linear networks: application to urban cycling profiles. *Stat*, 13 (4).
- Matthias, E. and Moradi, M. (2024). Marked spatial point processes: current state and extensions to point processes on linear networks. *Journal of Agricultural Biological and Environmental Statistics*, 29 (4):346–378.
- McDowall, D., Loftin, C., and Pate, M. (2011). Seasonal cycles in crime, and their variability. *Journal of Quantitative Criminology*, 28:389–410.
- McSwiggan, G., Baddeley, A., and Nair, G. (2017). Kernel density estimation on a linear network. *Scandinavian Journal of Statistics*, 44(2):324–345.
- Medvedovic, M. and Sivaganesan, S. (2002). Bayesian infinite mixture model based clustering of gene expression profiles. *Bioinformatics*, 18(9):1194–1206.

- Mohler, G. (2014). Marked point process hotspot maps for homicide and gun crime prediction in Chicago. *International Journal of Forecasting*, 30(3):491–497.
- Mohler, G. O., Short, M. B., Brantingham, P. J., Schoenberg, F. P., and Tita, G. E. (2011). Self-exciting point process modeling of crime. *Journal of the american statistical association*, 106(493):100–108.
- Moradi, M. M. and Mateu, J. (2020). First-and second-order characteristics of spatio-temporal point processes on linear networks. *Journal of Computational and Graphical Statistics*, 29(3):432–443.
- Okabe, A. and Sugihara, K. (2012). *Spatial analysis along networks: statistical and computational methods*. John Wiley & Sons.
- Park, J., Schoenberg, F. P., Bertozzi, A. L., and Brantingham, P. J. (2021). Investigating clustering and violence interruption in gang-related violent crime data using spatial-temporal point processes with covariates. *Journal of the American Statistical Association*, 116(536):1674–1687.
- Park, J., Yi, S., Chang, W., and Mateu, J. (2023). A spatio-temporal dirichlet process mixture model for coronavirus disease-19. *Statistics in Medicine*, 42(30):5555–5576.
- Quick, H., Holan, S. H., Wikle, C. K., and Reiter, J. P. (2015). Bayesian marked point process modeling for generating fully synthetic public use data with point-referenced geography. *Spatial Statistics*, 14:439–451.
- R Core Team (2022). *R: A Language and Environment for Statistical Computing*. R Foundation for Statistical Computing, Vienna, Austria.
- Rakshit, S., Baddeley, A., and Nair, G. (2019a). Efficient code for second order analysis of events on a linear network. *Journal of Statistical Software*, 90(1):1–37.
- Rakshit, S., Davies, T., Moradi, M. M., McSwiggan, G., Nair, G., Mateu, J., and Baddeley, A. (2019b). Fast kernel smoothing of point patterns on a large network using two-dimensional convolution. *International Statistical Review*, 87(3):531–556.

- Reich, B. J. and Bondell, H. D. (2011). A spatial dirichlet process mixture model for clustering population genetics data. *Biometrics*, 67(2):381–390.
- Reinhart, A. (2018). A review of self-exciting spatio-temporal point processes and their applications. *Statistical Science*, 33(3):299–318.
- Santitissadeekorn, N., Short, M. B., and Lloyd, D. J. B. (2018). Sequential data assimilation for 1d self-exciting processes with application to urban crime data. *Computational Statistics and Data Analysis*, 128:163–183.
- Scott, D. W. (2015). *Multivariate density estimation: theory, practice, and visualization*. John Wiley & Sons.
- Sethuraman, J. (1994). A constructive definition of dirichlet priors. *Statistica sinica*, pages 639–650.
- Song, J., Spicer, V., and Brantingham, P. (2013). The edge effect: Exploring high crime zones near residential neighborhoods. In *2013 IEEE International Conference on Intelligence and Security Informatics*, pages 245–250.
- Stucky, T. D. and Ottensmann, J. R. (2009). Land use and violent crime. *Criminology*, 47:1009–1368.
- Taddy, M. A. (2010). Autoregressive mixture models for dynamic spatial poisson processes: Application to tracking intensity of violent crime. *Journal of the American Statistical Association*, 105(492):1403–1417.
- Weisburd, D. L. (2018). Hot spots of crime and place-based prevention. *Criminology & Public Policy*, 17:5–25.
- Wilcox, P. and Eck, J. E. (2011). Criminology of the unpopular: Implications for policy aimed at payday lending facilities. *Criminology & Public Policy*, 10:473–482.
- Zhang, X., Liu, L., Lan, M., Song, G., Xiao, L., and Chen, J. (2022). Interpretable machine learning models for crime predictiony. *Computers, Environment and Urban Systems*, 94:101789.

Zhuang, J. and Mateu, J. (2019). A semiparametric spatiotemporal hawkes-type point process model with periodic background for crime data. *Journal of the Royal Statistical Society Series A: Statistics in Society*, 182(3):919–942.